



Geophysical Research Letters°

RESEARCH LETTER

10.1029/2022GL100555

Key Points:

- Enhanced ionospheric irregularities with highly variable velocities were observed after the Tonga volcanic eruption
- The maximum amplitude of the line-of-sight velocity of the ionospheric oscillation approached 150 m/s in E layer
- The ionosphere was displaced upward by as much as 100 km

Supporting Information:

Supporting Information may be found in the online version of this article.

Correspondence to:

J. Zhang, jjzhang@spaceweather.ac.cn

Citation:

Zhang, J., Xu, J., Wang, W., Wang, G., Ruohoniemi, J. M., Shinbori, A., et al. (2022). Oscillations of the ionosphere caused by the 2022 Tonga volcanic eruption observed with SuperDARN radars. *Geophysical Research Letters*, 49, e2022GL100555. https://doi.org/10.1029/2022GL100555

Received 26 JUL 2022 Accepted 12 OCT 2022

Author Contributions:

Conceptualization: Jiaojiao Zhang, Jiyao Xu

Data curation: Xiang Deng, Ailan Lan Funding acquisition: Jiaojiao Zhang, Chi Wang

Investigation: Jiyao Xu, Atsuki Shinbori, Nozomu Nishitani, Chi Wang, Jingye Yan Methodology: Jiaojiao Zhang

Project Administration: Chi Wang **Software:** Jiaojiao Zhang, J. Michael Ruohoniemi

Supervision: Jiyao Xu, Chi Wang Validation: Jiaojiao Zhang, Wei Wang, Guojun Wang

Visualization: Jiaojiao Zhang Writing – original draft: Jiaojiao Zhang Writing – review & editing: Jiaojiao Zhang, J. Michael Ruohoniemi

© 2022. American Geophysical Union. All Rights Reserved.

Oscillations of the Ionosphere Caused by the 2022 Tonga Volcanic Eruption Observed With SuperDARN Radars

Jiaojiao Zhang^{1,2} , Jiyao Xu^{1,2} , Wei Wang^{1,2} , Guojun Wang^{1,2} , J. Michael Ruohoniemi³ , Atsuki Shinbori⁴ , Nozomu Nishitani⁴ , Chi Wang^{1,2} , Xiang Deng¹ , Ailan Lan^{1,2} , and Jingye Yan^{1,2}

¹State Key Laboratory of Space Weather, National Space Science Center, Chinese Academy of Sciences, Beijing, China, ²University of Chinese Academy of Sciences, Beijing, China, ³Center for Space Science and Engineering Research (Space@VT), Virginia Polytechnic Institute and State University, Blacksburg, VA, USA, ⁴Institute for Space-Earth Environmental Research, Nagoya University, Nagoya, Japan

Abstract On 15 January 2022, the submarine volcano on the southwest Pacific island of Tonga violently erupted. Thus far, the ionospheric oscillation features caused by the volcanic eruption have not been identified. Here, observations from the Super Dual Auroral Radar Network radars and digisondes were employed to analyze ionospheric oscillations in the Northern Hemisphere caused by the volcanic eruption in Tonga. Due to the magnetic field conjugate effect, the ionospheric oscillations were observed much earlier than the arrival of surface air pressure waves, and the maximum negative line-of-sight (LOS) velocity of the ionospheric oscillations exceeded 100 m/s in the F layer. After the surface air pressure waves arrived, the maximum LOS velocity in the E layer approached 150 m/s. A maximum upward displacement of 100 km was observed in the ionosphere. This work provides a new perspective for understanding the strong ionospheric oscillation caused by geological hazards observed on Earth.

Plain Language Summary On 15 January 2022, an underwater volcano on the southwest Pacific island of Tonga erupted, triggering significant disturbances on the surface and in the ionosphere that propagated worldwide. The oscillation features of the ionosphere caused by the volcanic eruption have not been identified. The volcanic eruption caused numerous irregularities in the ionosphere. These irregularities move with the ionosphere similar to how leaves move in a rough sea. In this study, the ionospheric irregularities were observed and employed as tracers to analyze the ionospheric oscillations. Different features of ionospheric oscillations, including the maximum line-of-sight (LOS) velocity, the altitude of the maximum LOS velocity, and the propagation direction, were observed before and after the arrival of the surface air pressure waves. The amplitudes of the LOS velocities of the ionospheric fluctuations approached 150 m/s, and a maximum upward displacement of 100 km, which is the strongest ionospheric fluctuation caused by geological hazards ever observed.

1. Introduction

At 04:14:45 UTC on 15 January 2022, the Hunga Tonga-Hunga Ha'apai submarine volcano (hereafter referred to as the Tonga volcano), which is centered at 20.546°S, 175.390°W, explosively erupted. Immense ripples on the sea surface and in the atmosphere rapidly spread outward. The volcanic explosivity index (VEI) was estimated to be 6, indicating that this eruption was one of the largest volcanic eruptions recorded in the modern era (Poli & Shapiro, 2022). The volcanic eruption released a large amount of material and energy into the atmosphere, with the highest overshooting tops of the volcanic plume reaching the lower mesosphere at an altitude of ~55 km according to satellite imagery (Carr et al., 2022). The waves triggered by the Tonga volcanic eruption on the surface and in the ionosphere were observed worldwide by various ground- and space-based instrumentation (Adam, 2022; X. Liu et al., 2022; Wright et al., 2022).

It is well known that volcanic eruptions and earthquakes can produce measurable ionospheric waves that travel thousands of kilometers (Meng et al., 2019; Roberts et al., 1982). Previous studies on ionospheric disturbances caused by volcanic eruptions, earthquakes, or tsunamis mainly involved total electron content (TEC) variations and horizontal phase velocities of the waves (Dautermann et al., 2009; Heki, 2006; Huang et al., 2019; C. H. Liu et al., 1982). Studies on direct observations of the ionospheric oscillation velocity or amplitude caused by these natural hazards are rare (Nishitani et al., 2011). After the Tonga volcanic eruption, the dense Global

Navigation Satellite System receiver network was selected to rapidly analyze the TEC perturbations associated with the volcanic eruption. Themens et al. (2022) identified two large-scale traveling ionospheric disturbances (LSTIDs) with initial speeds of 950 m/s and 555 m/s. The two LSTIDs exhibited strong directionality and slowed down substantially with radial distance. Flowing the two LSTIDs, medium-scale TIDs (MSTIDs) with speeds of 200–400 m/s were observed and propagated globally. Zhang et al. (2022) discovered that the radial two-way disturbance propagation along the entire great circle lasted 4 days. This observation showed that the waves traveled around the globe three times as Lamb waves with primary speeds in the range of 300–350 m/s. Lin et al. (2022) observed the simultaneous occurrence of concentric TIDs (CTIDs) in Australia and Japan between 0800 and 1000 universal time (UT) on 15 January 2022. CTIDs observed in Japan were attributed to the magnetic field conjugate effect. The authors explained that the polarization electric field originated from an E-region dynamo driven by atmospheric disturbance waves in the Southern Hemisphere can be transmitted to magnetically conjugate regions in the Northern Hemisphere along conductive geomagnetic field lines with Alfvenic speed (300 km/s), which is much faster than the speed of Lamb waves. The external electric field, which originated from the conjugate hemisphere generated the CTIDs observed in Japan. Shinbori et al. (2022) studied the electromagnetic conjugate effect of ionospheric disturbances after the Tonga volcanic eruption by using observations

Field-aligned electron density irregularities are small-scale density structures in the ionospheric plasma. When the ionosphere fluctuates, these structures move with the ionosphere. Thus, ionospheric irregularities are good tracers for ionospheric movement. SuperDARN radars are powerful tools for observing the motion of irregularities in the ionosphere (Chisham et al., 2007; Nishitani et al., 2019). In this study, ionospheric irregularities observed by using mid-latitude SuperDARN radars and digisondes were employed as tracers to study ionospheric oscillation features in the Northern Hemisphere. It is very interesting that there were different ionospheric oscillation features, such as the maximum LOS velocity and the altitude of the maximum LOS velocity, before and after the arrival of the surface air pressure waves, indicating that the mechanisms of ionospheric oscillations were different in the two stages. In particular, the observations also revealed a significant vertical oscillation of the ionosphere caused by the volcanic eruption.

from the GNSS-TEC and Super Dual Auroral Radar Network (SuperDARN) Hokkaido radars, which further confirmed the explanation by Lin et al. (2022). However, the Tonga volcanic eruption effects on ionospheric

oscillations, especially in the vertical direction, have not been well demonstrated.

2. Data

SuperDARN is a global high frequency (HF), coherent scatter radar network that consists of more than 30 radars that observe Earth's upper atmosphere beginning at mid-latitudes and extending to polar regions in both hemispheres. There are now 37 SuperDARN radars, with 22 radars located in high-latitude and polar regions and 15 radars located in mid-latitude regions. The SuperDARN radars are sensitive to Bragg scattering from field-aligned electron density irregularities in the ionosphere (Greenwald et al., 1995). These radars operate in the HF band of the radio spectrum between 8 and 20 MHz; at these frequencies, radar signals are refracted by the ionosphere. The signals return to the radar along the same path, with the incident radar signal orthogonal to the magnetic field. The scale size of the irregularities from which the signal is scattered is equal to one-half of the radar wavelength. The HF signals are refracted toward the ground, and part of the signal may be reflected to the radar. Therefore, in addition to the backscatter received from ionospheric irregularities, SuperDARN radars receive backscatter from the ground or sea surface. The transmission of a multipulse scheme is used to calculate autocorrelation functions (ACFs) of the backscattered signals as a function of range. In each range gate, the ACF is analyzed by a fitting routine known as FITACF that estimates the backscatter power, the LOS Doppler velocity of the irregularities and the spectral width (Ribeiro et al., 2013). A typical SuperDARN radar monitors 16 or 24 beam directions separated by 3.24° in the azimuthal direction, with the 75 \sim 100 range gates along each beam separated by 45 km. The dwell time of each beam is typically $2 \sim 7$ s (integration period), which produces a $1 \sim 2$ min azimuthal scan.

The high-latitude SuperDARN radars are mainly employed to research the ionospheric convection driven by solar wind and magnetospheric interactions. Compared with radars located in high latitudes, mid-latitude radars are more suitable for research on sub-auroral phenomena and ion-neutral interactions, for example, TIDs. During the volcanic eruption in Tonga, data from four mid-latitude SuperDARN radars were available. These radars included the Jiamusi radar (JME) in China (geographic coordinates of 46.816°N, 130.402°E), the Hokkaido East radar (HOK) (geographic coordinates of 43.53°N, 143.61°E), the Hokkaido West radar (HKW) in Japan (geographic

ZHANG ET AL. 2 of 9

19448007, 2022, 20, Downloaded from https://agupubs.onlinelibrary.wiley.com/doi/10.1029/2022GL100555, Wiley Online Library on [12/05/2023]. See the Terms and Conditions

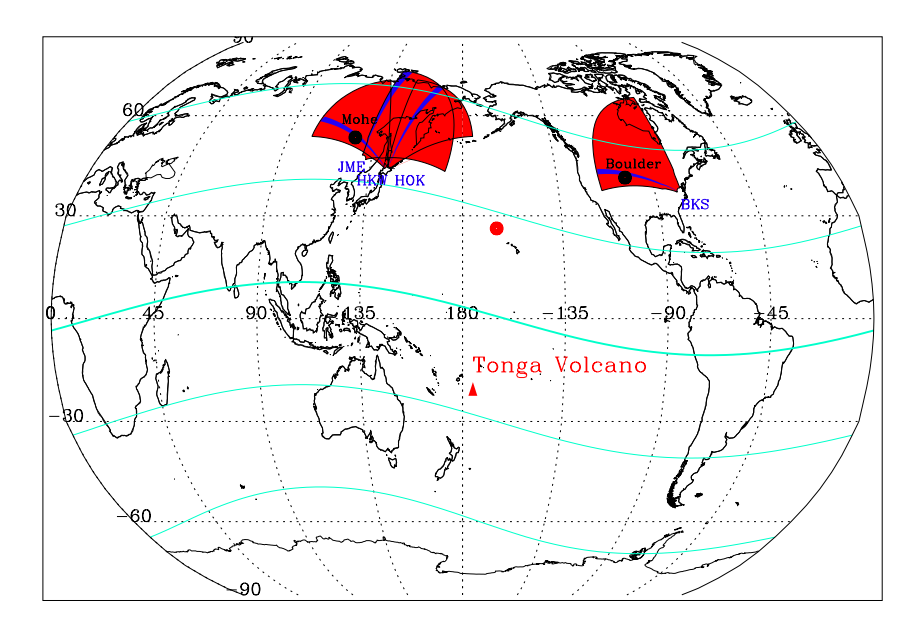


Figure 1. Fields of views (FOVs) of the Super Dual Auroral Radar Network Jiamusi (JME), Hokkaido East (HOK), Hokkaido West (HKW), and Blackstone (BKS) radars, where, beam 0 of the JME radar and beam 4 of the HOK, HKW, and BKS radars are shaded in blue. The black dots represent the locations of the Mohe and Boulder digisondes. The red triangle indicates the location of the Tonga volcano, and the red dot indicates the magnetically conjugate point of the volcano. The cyan curves indicate the magnetic latitude lines with 30° intervals.

coordinates of 43.54°N, 143.61°E), and the Blackstone radar (BKS) in the United States (geographic coordinates of 37.10°N, 77.95°W). Observations from these four radars were used to analyze the ionospheric oscillations in this study. The fields of view (FOVs) of the four radars are shown in Figure 1, where beam 0 of the JME radar and beam 4 of the HOK, HKW, and BKS radars are shown in blue. Beam 0 is the east-most beam of these four radars. The JME and BKS radars have 24 beams, while the HOK and HKW radars have 16 beams. On 15 January 2022, all four radars were operating in normal (fast) mode, and sequentially sampled beams with a 2–3 s integration time for each beam; thus, the whole FOV was sampled every minute. The operating frequencies of the HOK, HKW, and JME radars on 15 January 2022 were 11.07 MHz, 10.08 MHz, and 10.4 MHz, respectively. The operating frequency of the BKS radar was 10.8 MHz before 1300 UT and 11.5 MHz after 1300 UT.

The SuperDARN radars are used to observe the LOS velocities of plasma. In addition to the SuperDARN radar data, ionogram data from two digisondes located in Mohe, Heilongjiang, China (geographic coordinates of 52.0°N, 122.52°E) and Boulder, Colorado, USA (geographic coordinates of 40.0°N, 105.3°W) were used to investigate the height variations in the ionosphere. The densities and heights of the peaks of layers E, Es, F1, and F2 and electron density profiles up to 1,000 km can be automatically calculated by digisondes. The Mohe ionogram data were obtained from the Chinese Meridian Project Database, and the Boulder ionogram data were obtained from the Digital Ionogram Database (Reinisch & Galkin, 2011).

3. Results

3.1. LOS Velocity Observed by the Four SuperDARN Radars

Range-time-intensity (RTI) plots of the LOS Doppler velocities observed by (a) beam 4 of the HOK radar, (b) beam 0 of the JME radar, (c) beam 4 of the HKW radar and (d) beam 4 of the BKS radar on 15 January 2022 are shown in Figure 2. The LOS Doppler velocities are scaled according to the color bar shown on the right. Negative velocities represent plasma flows moving away from the radar, while positive velocities represent plasma flows moving toward the radar. The slant range is the total distance traversed by the ray between the radar and the targets. The shadow in each panel indicates night. As shown in Figure 1, beam 0 of the JME radar points to the geographical North Pole, beam 4 of the HOK radar is almost parallel to beam 0 of the JME radar, and beam 4 of the HKW and BKS radars points westward.

ZHANG ET AL. 3 of 9

19448007, 2022, 20, Downloaded from https://agupubs.onlinelibrary.wiley.com/doi/10.1029/2022GL100555, Wiley Online Library on [12/05/2023]. See the Terms and Conditions (https://onlinelibrary.wiley.com/term

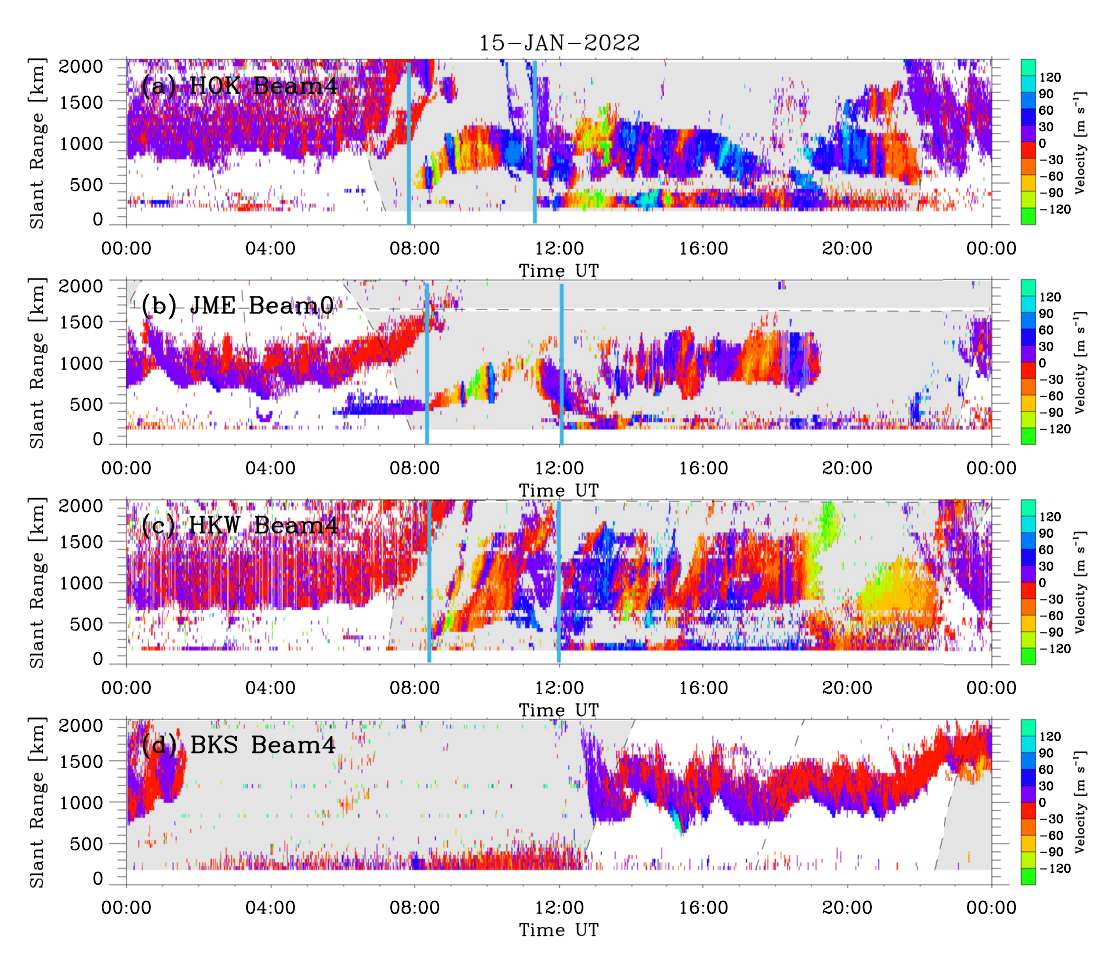


Figure 2. Range-time-intensity plots of the line-of-sight (LOS) Doppler velocities observed by (a) beam 4 of the Hokkaido East (HOK) radar, (b) beam 0 of the Jiamusi (JME) radar, (c) beam 4 of the Hokkaido West (HKW) radar and (d) beam 4 of the Blackstone (BKS) radar on 15 January 2022. The LOS Doppler velocities are scaled according to the color bar shown on the right. The shadow in each panel indicates night. The two blue vertical lines in (a, b, c) indicates the arrival time of the two groups of oscillations.

Before 0800 UT, backscatter with LOS velocities of less than ±30 m/s was observed by beam 4 of the HOK radar and classified as ground backscatter. Distinct ionospheric backscatter began to be observed from 0800 UT on beam 4 of the HOK radar. Plasma with negative LOS velocities were observed first, with a minimum of approximately -100 m/s, followed by a very short positive LOS velocity period with a maximum of approximately 60 m/s. Subsequently, a second sudden transition structure with a negative LOS velocity was captured; this was followed by a short positive LOS velocity period, with velocity more rapid than the previous velocity. At 0900 UT, the third negative velocity period, which lasted approximately 1 hour, with slower velocities than the second period, was observed. From 0800 UT to 1000 UT, the location of the echoes gradually moved to a further slant range. After 1000 UT, positive velocities were observed by the radars, and the location of the echoes gradually decreased to a closer slant range until 1130 UT. Beam 0 of the JME radar was approximately 1,100 km west of beam 4 of the HOK radar, and the two beams were nearly parallel to each other. Similar ionospheric oscillation features with some time delay were observed from beam 4 of the HOK radar. As shown in Figure 2b, from 0900 UT to 1200 UT, three negative/positive velocity periods, with a relatively short duration for the first two positive velocity periods (10 min), were observed by the JME radar. The second negative/positive velocity period between 0920 UT and 1020 UT was the most rapid. The slant range of the observed echoes slowly increased from 0900 UT at approximately 500 km and rapidly dropped from a slant range of more than 1,000 km at 1100 UT to a few hundred kilometers. Beam 4 of the HKW radar points westward. Figure 2c shows that the observations from beam 4 of the HKW radar are consistent with the observations from the HOK and JME radars. The positive LOS velocity regions moved to a farther slant range over time, indicating the westward propagation of the fluctuation.

ZHANG ET AL. 4 of 9

Before 1120 UT, few backscatter in the slant range between 200 and 400 km (E layer of the ionosphere based on ray tracing simulations, please refer to Figure S1 in the Supporting Information S1) were observed by beam 4 of the HOK radar. The magnitudes of the LOS velocities in this slant range were weaker than those in the slant range greater than 400 km (F layer of the ionosphere). According to data from surface pressure stations, Wright et al. (2022) identified surface air pressure propagated as a Lamb wave at a phase speed of 318.2 ± 6 m/s Shinbori et al. (2022) showed that the surface air pressure waves propagated to Japan at around 1120 UT as Lamb mode waves based on the thermal infrared grid data observed by the Himawari 8 satellite. After 1120 UT, much backscatter appeared in the E region of the ionosphere and were observed by the HOK radar; the LOS velocities in the E layer exceeded ± 150 m/s and were stronger than those in the F region between 1120 UT and 1600 UT. After 1200 UT, the JME and HKW radars also observed an increase in the number of ionospheric echoes in the E layer.

According to the observations from the HOK and JME radars between 0800 UT and 1200 UT, the propagation direction of the ionospheric oscillation was westward. After the arrival of the surface air pressure waves, the propagation direction turned northwestward. Figure S2 in the Supporting Information S1 show the wavefronts observed by the HOK and JME radars at 0850, 0940 and 1133 UT. The horizontal phase velocity was approximately 330 m/s, which was calculated by using the delay time and the distance between the HOK radar and the JME radar. The propagation direction and horizontal phase velocity of the ionospheric fluctuations observed by the SuperDARN radars were consistent with the observations based on the TEC (Lin et al., 2022), which indicates that this group of oscillations was due to magnetic conjugate effect. Shinbori et al. (2022) also showed that the LOS Doppler velocity observed by the SuperDARN HOK was associated with the passage of TEC perturbations due to magnetic conjugate effect. Strong ionospheric oscillations were observed by the SuperDARN radars in East Asia, with three LOS velocity transitions from 0800 UT to 1200 UT that may be attributed to the three main explosions of the volcanic eruptions in Tonga (Astafyeva et al., 2022; Wright et al., 2022). During this period, the slant range of the echoes showed a trend of rising, falling, and then rising, implying variations in the height of the ionosphere in addition to oscillations in the horizontal direction.

The BKS radar is located in the Western Hemisphere and under different day-night conditions during the period of interest. The backscatter received by the BKS radar was considerably different from the backscatter received by the other three radars. Almost all of the backscatter was ground scatter. The velocity variation in ground scatter for the SuperDARN radars is usually attributed to vertical movement of the ionosphere. The BKS radar received minimal backscatter before 1200 UT as the radar operating frequency and ionospheric conditions were not suitable. With sunrise, the ionosphere builds up and a band of ground scatter developed after 1230 UT. The slant range to the band varies and the LOS velocity fluctuates within narrow limits (<30 m/s) throughout the day owing to passage of TIDs, which is typical. However, after 1400 UT, ground scatter with LOS velocities greater than 90 m/s was observed by beam 4 of the BKS radar, corresponding to a marked downward motion in the ionosphere. Figure S3 in the Supporting Information S1 shows the radar observations at 1440, 1445, and 1450 UT. This figure clearly shows the downward motion of the ionosphere propagating northeastward. We estimated that the propagation velocity of the ionospheric fluctuation was approximately 320 m/s.

3.2. LOS Velocity Across Different Layers of Ionosphere

To show the fluctuation velocity across different layers of the ionosphere, Figure 3 shows an RTI plot of the LOS Doppler velocity observed by beam 4 of the HOK radar and line plots of the LOS velocities of range gates 2, 4, 10, 12, 14, and 16 for beam 4 of the HOK radar, with 10 min smoothing applied. The positive/negative velocities indicate that the direction of the LOS velocity was toward/away from the radar. Range gates 2, 4, 10, 12, 14, and 16 correspond to slant ranges of 270, 360, 630, 720, 810, and 900 km, as indicated by the six black horizontal lines on Figure 3a. The blue vertical line at 0800 UT indicates the arrival time of the disturbance propagated from the magnetic conjugate point of the Tonga volcanic eruption, while the blue vertical line at 1120 UT indicates the arrival time of the disturbance directly propagated from the Tonga volcanic eruption. Between 0800 UT and 1120 UT, the maximum peak-to-peak amplitude of the ionospheric fluctuation velocity was approximately 150 m/s at range gate 10 (F layer) and was associated with the two shock structures. During this period, the peak-to-peak amplitude observed at gate 2 (E layer) was weaker than that observed in the F layer. After the arrival of the surface air pressure waves at around 1120 UT, the maximum LOS velocity was approximately ±150 m/s, and the peak-to-peak amplitude of the ionospheric fluctuation approached 300 m/s at range gate 4 (E layer). The peak-to-peak amplitude decreased over time and as the range gate increased.

ZHANG ET AL. 5 of 9

19448007, 2022, 20, Downloaded from https://agupubs.

onlinelibrary wiley com/doi/10.1029/2022GL100555, Wiley Online Library on [12/05/2023]. See the Terms and Conditions (https:/

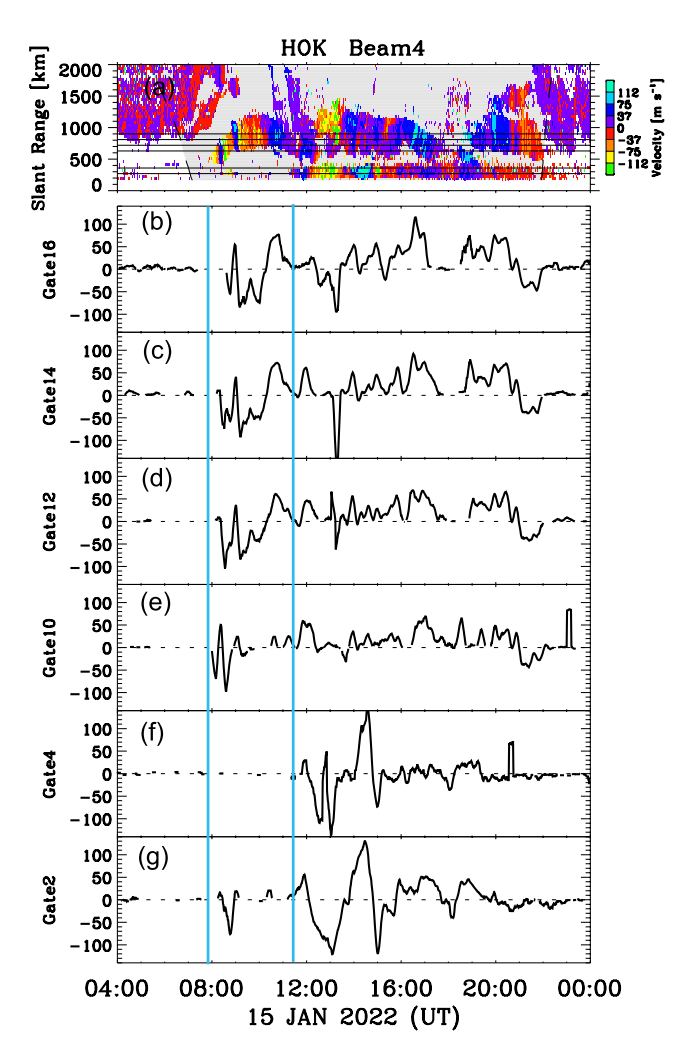


Figure 3. Fluctuation velocity across different layers of the ionosphere. (a) Range-time-intensity plot of the line-of-sight (LOS) Doppler velocities observed by beam 4 of the Hokkaido East (HOK) radar and line plots of the LOS velocities of range gates (b) 16, (c) 14, (d) 12, (e) 10, (f) 4 and (g) 2 for beam 4 of the HOK radar, with 10 min smoothing applied. Range gates 2, 4, 10, 12, 14 and 16 correspond to slant ranges of 270, 360, 630, 720, 810, and 900 km, respectively, as indicated by the six black horizontal lines in Figure 4a. The two vertical blue lines indicate the arrival time of the disturbance from the magnetic conjugate point of the volcanic eruption in Tonga and from the volcanic eruption itself.

3.3. Uplift in the Ionosphere by the Volcanic Eruption

The SuperDARN radars observed the LOS velocity of the irregularities. To investigate the vertical motion of the ionosphere, we combined the observations from beam 4 of the HKW radar and Mohe digisonde. Beam 4 of the HKW radar and the location of the Mohe digisonde are shown in Figure 1. Figure 4 shows the RTI plot of the LOS Doppler velocities observed by beam 4 of the HOK radar, the F layer peak height (hmF2) as a function of time obtained from the Mohe digisonde, and three representative ionograms to highlight the state of the ionosphere at specific times. The black horizontal dashed line in Figure 4a indicates the radar slant range corresponding to the Mohe digisonde. The two vertical blue lines in Figures 4a and 4b indicate the arrival time of the disturbance to the Mohe digisonde from the magnetic conjugate point of the volcanic eruption in Tonga at 0930 UT and from the volcanic eruption itself at 1230 UT, respectively. The cyan dashed line in Figure 4b indicates the variation in the peak height of the F layer during the quiet time (polynomial fitting curve based on observations on 13 January 2022). As shown in Figure 4, the negative/positive LOS velocities of the HKW radar correspond to the upward/downward motion, respectively, of the ionosphere, which were captured by the Mohe digisonde, indicating that the LOS velocities observed by the SuperDARN radars have a pronounced vertical component and were not purely horizontal. After the arrival of the disturbance from the magnetic conjugate point of the volcanic eruption at 0930 UT, an uplift of the ionosphere from 245 km to about 326 km was observed by the Mohe digisonde at 1030 UT, and then the height of the ionosphere vibrated and fell to a normal height. After the disturbance from the volcanic eruption itself propagated to Mohe at approximately 1230 UT, the uplift of the ionosphere was again observed by the digisonde. Excluding the diurnal variation in the peak height of the F layer at the quiet time, the maximum amplitude of the vertical fluctuations caused by the volcanic eruption in Tonga was approximately 80 km, as observed by the Mohe digisonde. This finding indicates that the volcanic eruption caused strong vertical fluctuations of the ionosphere in the midlatitude region of the Northern Hemisphere. This vertical movement may be attributed to the fact that magnetic field lines in mid latitudes are not completely perpendicular to the ground; thus, east-west electric fields in this region will produce vertical movements of the ionosphere in addition to horizontal movements.

Joint observations from beam 4 of the BKS radar and Boulder digisonde also revealed the vertical oscillation of the ionosphere (see Figure S4 in the Supporting Information S1). The position of the Boulder digisonde is beyond the 2,000 km slant range of the BKS radar, so the location of the digisonde was not marked in the figure. A maximum positive velocity of approximately 90 m/s was observed by beam 4 of the BKS radar from 1400 UT, which

corresponds to a marked downward motion in the ionosphere. The Boulder digisonde also observed the rapid decrease in the peak height of the F layer from 1400 UT with an amplitude of more than 100 km, which is consistent with the observation from the BKS radar. The disturbance from the magnetic conjugate point of the volcanic eruption in Tonga and from the volcanic eruption itself arrived at the Boulder digisonde at 0905 UT and 1215 UT, respectively, which was calculated based on the speed of the Lamb wave.

4. Discussion and Conclusion

Figure S5 in the Supporting Information S1 shows the RTI plots of the LOS Doppler velocities observed by the four SuperDARN radars on 14 January 2022 and 15 January 2022 with the SYM-H index. It was noted that there was a moderate storm during 14–15 January 2022, with the SYM-H index dropping to –101 nT at 2217 UT on

ZHANG ET AL. 6 of 9

1944/8007, 2022, 20, Dowloladed from https://agupubs.onlinelibary.wiley.com/doi/10.1029/2023GL100555, Wiley Online Library on [12/05/2023]. See the Terms and Conditions (https://onlinelibrary.wiley.com/terms-and-conditions) on Wiley Online Library for rules of use; OA articles are governed by the applicable Creative Co.

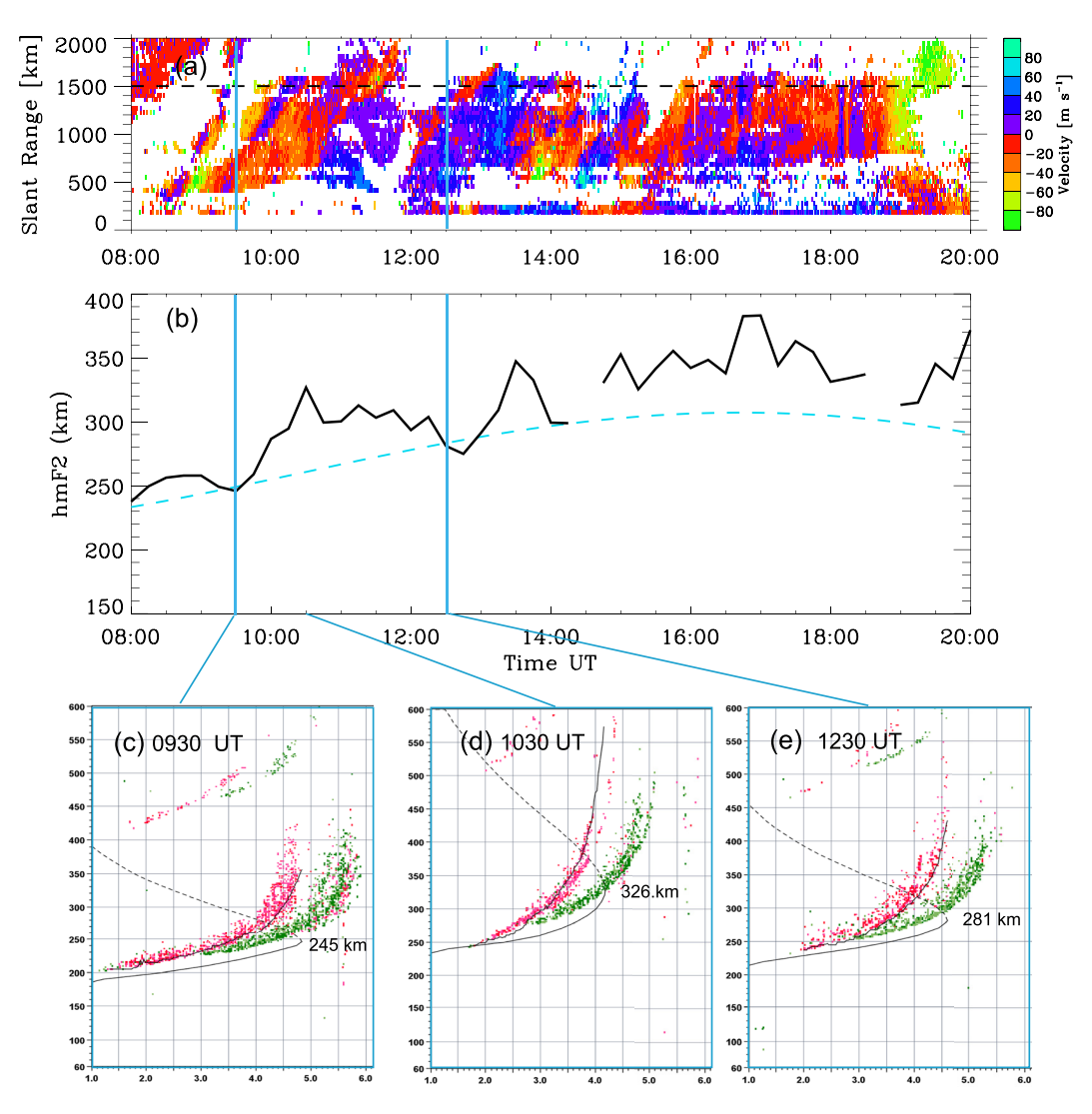


Figure 4. Vertical variation of the ionosphere. (a) Range-time-intensity plot of the line-of-sight (LOS) Doppler velocities observed by beam 4 of the Hokkaido East (HOK) radar. The black horizontal dashed line in panel (a) indicates the slant range corresponding to the Mohe digisonde. (b) Ionospheric peak height of the F2 layer as a function of time obtained from the Mohe digisonde. The two vertical blue lines in panel (a and b) indicate the arrival time of the disturbance to the Mohe digisonde from the magnetic conjugate point of the volcanic eruption in Tonga and from the volcanic eruption itself, respectively. The cyan dashed curve in panel (b) indicates the variation in the peak height of the F layer of the ionosphere during the quiet time. Three representative ionograms are shown at (c) 0930 UT, (d) 1045 UT, and (e) 1230 UT.

14 January 2022. Analyses by Lin et al. (2022) and Shinbori et al. (2022) showed that the interplanetary magnetic field Bz turned northward at 2330 UT on 14 January 2022, and the AE index remained at a very low level from 0400 UT to 1100 UT on 15 January 2022. When the eruption occurred, the storm was in the late recovery phase. Geomagnetic storms are known to generate LSTIDs that propagate from high latitudes to equatorward (e.g., Richmond, 1978, and others). The perturbations propagated westward and northwestward in East Asia and propagated northeastward in the United States. The propagation direction and velocity were different from the propagation feature of the storm-time LSTIDs, and they were consistent with the features of the TIDs caused by the volcanic eruption.

According to the observations from the SuperDARN radars in East Asia, the strongest LOS velocity appeared in the F layer of the ionosphere due to the magnetic field conjugate effect, and the amplitude of the velocity decreased with decreasing altitude. This finding indicates that the magnetic field conjugate effect has a significant impact on the plasma flow in the F layer in another hemisphere. During this period, the ionospheric plasma

ZHANG ET AL. 7 of 9

flow was produced by an external electric field that was generated by an E layer dynamo in the sunlit Southern Hemisphere. The two sudden increases of the plasma flow may correspond to the two large Tonga eruptions with VEI values of 6, which can cause a significant enhancement of an E-region dynamo electric field. After the arrival of surface air pressure waves, the strongest LOS velocity appeared in the E layer, and the amplitude of the velocity decreased with increasing altitude. During this period, the ionospheric conductivity of the E-region was very small due to the dark region, and the E layer dynamo process was not effective on the ionospheric plasma motion in the F-region. Thus, the E and F layer motions were directly produced by the neutral wind osculation associated with arrival of the air pressure waves. The collision frequency was much smaller in the F layer than in the E layer. Therefore, the plasma motion was expected to be slower in the F layer than in the E layer.

The fluctuation caused by the magnetic field conjugate effect was detected by three radars in East Asia, while the BKS radar in America did not record fluctuations caused by the magnetic field conjugate effect. This was attributed to the fact that the radar operating frequency and ionospheric conditions did satisfy the conditions for receiving ionospheric backscatter during the relevant period. In addition, the three midlatitude SuperDARN radars in Australia and New Zealand in the Southern Hemisphere were not operating during this period. If these radars were operational, they would have provided excellent observations for comparing movements in the ionosphere caused by volcanic eruptions in the Southern and Northern Hemispheres, and would have contributed to a deeper understanding of the mechanisms underlying the magnetic field conjugate effect.

In conclusion, impacts on ionospheric irregularities and ionospheric oscillation features in the Northern Hemisphere caused by the explosive Tonga volcanic eruption in the southwest Pacific were clearly captured by midlatitude SuperDARN radars and digisondes. The ionospheric fluctuations observed by SuperDARN radars in East Asia propagated westward due to the magnetic field conjugate effect. After the surface pressure waves arrived, the propagation direction was northwestward. The distant and upward motions of the ionosphere was considerably more rapid and lasted longer than the forward and downward motions. Because of different mechanisms, the maximum peak-to-peak LOS velocity of the ionosphere exceeded 150 m/s appeared in F layer due to the magnetic field conjugate effect, and the maximum peak-to-peak LOS velocity of the ionosphere was approximately 300 m/s and appeared in the E layer due to the direct propagation of the wave from the Tonga volcano. The amplitude of the vertical rise and fall of the ionosphere in the mid-latitude region of the Northern Hemisphere reached nearly 100 km due to the volcanic eruption. This event shows how geological hazards can impact the ionosphere and cause space weather, raising concerns for vulnerable technologies.

Data Availability Statement

The raw SuperDARN data are available from the SuperDARN data server at the National Space Science Center, Chinese Academy of Sciences (https://superdarn.nssdc.ac.cn/). To access the data, users should log in, and go to "Access data" to select the radar, data set and date. The Mohe ionogram data were obtained from the Chinese Meridian Project Database (https://data.meridianproject.ac.cn/), to access the data, users also should log in, and go to "Download," then select "Mohe station," and then choose "Ionogram image of digital ionosonde." The Boulder ionogram data were obtained from the Digital Ionogram Database (http://spase.info/SMWG/Observatory/GIRO). The SYM-H index can be downloaded from World Data Center for Geomagnetism, Kyoto (https://doi.org/10.14989/267216).

Acknowledgments

This work was supported by National Natural Science Foundation of China (NNSFC) Grants 41731070, 42174210, and 42188101. This work was also supported by the Key Research Program of Frontier Sciences CAS Grant. QYZDJ-SSW-JSC028 and the Specialized Research Fund for the State Key Laboratories of China. We also acknowledge the Chinese Meridian Project.

References

Adam, D. (2022). Tonga volcano eruption created puzzling ripples in Earths atmosphere. *Nature*, 602(7894), 497. https://doi.org/10.1038/d41586-022-00127-1

Astafyeva, E., Maletckii, B., Mikesell, T. D., Munaibari, E., Ravanelli, M., Coisson, P., et al. (2022). The 15 January 2022 Hunga Tonga eruption history as inferred from ionospheric observations. *Geophysical Research Letters*, 49(10), e2022GL098827. https://doi.org/10.1029/2022GL098827

Carr, J. L., Horvth, k., Wu, D. L., & Friberg, M. D. (2022). Stereo plume height and motion retrievals for the record-setting hunga Tonga-hunga ha'apai eruption of 15 January 2022. *Geophysical Research Letters*, 49(9), e2022GL098131. https://doi.org/10.1029/2022GL098131

Chisham, G., Lester, M., Milan, S. E., Freeman, M., Bristow, W., Grocott, A., et al. (2007). A decade of the super dual auroral radar network (superdarn): Scientific achievements, new techniques and future directions. *Surveys in Geophysics*, 28(1), 33–109. https://doi.org/10.1007/s10712-007-9017-8

Dautermann, T., Calais, E., & Mattioli, G. S. (2009). Global positioning system detection and energy estimation of the ionospheric wave caused by the 13 July 2003 explosion of the Soufrire hills volcano, Montserrat. *Journal of Geophysical Research*, 114(B2), B02202. https://doi.org/10.1029/2008JB005722

ZHANG ET AL. 8 of 9

- Greenwald, R. A., Baker, K. B., Dudeney, J. R., Pinnock, M., Jones, T. B., Thomas, E. C., et al. (1995). Darn/superdarn. *Space Science Reviews*, 71(1), 761–796. https://doi.org/10.1007/BF00751350
- Heki, K. (2006). Explosion energy of the 2004 eruption of the Asama volcano, central Japan, inferred from ionospheric disturbances. *Geophysical Research Letters*, 33(14), L14303. https://doi.org/10.1029/2006GL026249
- Huang, C. Y., Helmboldt, J. F., Park, J., Pedersen, T. R., & Willemann, R. (2019). Ionospheric detection of explosive events. Reviews of Geophysics, 57(1), 78–105. https://doi.org/10.1029/2017RG000594
- Lin, J.-T., Rajesh, P. K., Lin, C. C. H., Chou, M.-Y., Liu, J.-Y., Yue, J., et al. (2022). Rapid conjugate appearance of the giant ionospheric lamb wave signatures in the northern hemisphere after Hunga-Tonga volcano eruptions. *Geophysical Research Letters*, 49(8), e2022GL098222. https://doi.org/10.1029/2022GL098222
- Liu, C. H., Klostermeyer, J., Yeh, K. C., Jones, T. B., Robinson, T., Holt, O., et al. (1982). Global dynamic responses of the atmosphere to the eruption of mount St. Helens on 18 May 1980. *Journal of Geophysical Research*, 87(A8), 6281–6290. https://doi.org/10.1029/JA087iA08p06281
- Liu, X., Xu, J., Yue, J., & Kogure, M. (2022). Strong gravity waves associated with Tonga volcano eruption revealed by Saber observations. Geophysical Research Letters, 49(10), e2022GL098339. https://doi.org/10.1029/2022GL098339
- Meng, X., Vergados, P., Komjathy, A., & Verkhoglyadova, O. (2019). Upper atmospheric responses to surface disturbances: An observational perspective. *Radio Science*, 54(11), 1076–1098. https://doi.org/10.1029/2019RS006858
- Nishitani, N., Ogawa, T., Otsuka, Y., Hosokawa, K., & Hori, T. (2011). Propagation of large amplitude ionospheric disturbances with velocity dispersion observed by the superdarn Hokkaido radar after the 2011 off the Pacific coast of Tohoku earthquake. Earth Planets and Space, 63(7), 891–896. https://doi.org/10.5047/eps.2011.07.003
- Nishitani, N., Ruohoniemi, J. M., Lester, M., Baker, J. B. H., Koustov, A. V., Shepherd, S. G., et al. (2019). Review of the accomplishments of mid-latitude super dual auroral radar network (superdarn) hf radars. *Progress in Earth and Planetary Science*, 6(1), 27. https://doi.org/10.1186/s40645-019-0270-5
- Poli, P., & Shapiro, N. M. (2022). Rapid characterization of large volcanic eruptions: Measuring the impulse of the Hunga Tonga Haapai explosion from teleseismic waves. Geophysical Research Letters, 49(8), e2022GL098123. https://doi.org/10.1029/2022GL098123
- Reinisch, B. W., & Galkin, I. A. (2011). Global ionospheric radio observatory (giro). Earth Planets and Space, 63(4), 377–381. https://doi.org/10.5047/eps.2011.03.001
- Ribeiro, A., Ruohoniemi, J., Ponomarenko, P., Clausen, L., Baker, J., Greenwald, R., et al. (2013). A comparison of superdarn acf fitting methods. Radio Science, 48, 274–282. https://doi.org/10.1002/rds.20031
- Richmond, A. D. (1978). Gravity wave generation, propagation, and dissipation in the thermosphere. *Journal of Geophysical Research*, 83(A9), 4131–4145. https://doi.org/10.1029/JA083iA09p04131
- Roberts, D. H., Klobuchar, J. A., Fougere, P. F., & Hendrickson, D. H. (1982). A large-amplitude traveling ionospheric disturbance produced by the 18 May 1980, explosion of Mount St. Helens. *Journal of Geophysical Research*, 87(A8), 6291–6301. https://doi.org/10.1029/JA087iA08p06291
- Shinbori, A., Otsuka, Y., Sori, T., Nishioka, M., Perwitasari, S., Tsuda, T., & Nishitani, N. (2022). Electromagnetic conjugacy of ionospheric disturbances after the 2022 Hunga Tonga-Hunga Haapai volcanic eruption as seen in GNSS-TEC and superdarn Hokkaido pair of radars observations. Earth Planets and Space, 74(1), 106. https://doi.org/10.1186/s40623-022-01665-8
- Themens, D. R., Watson, C., Žagar, N., Vasylkevych, S., Elvidge, S., McCaffrey, A., et al. (2022). Global propagation of ionospheric disturbances associated with the 2022 Tonga volcanic eruption. Geophysical Research Letters, 49(7), e2022GL098158. https://doi.org/10.1029/2022GL098158
- Wright, C. J., Hindley, N. P., Alexander, M. J., Barlow, M., Hoffmann, L., Mitchell, C. N., et al. (2022). Surface-to-space atmospheric waves from Hunga Tonga-Hunga Haapai eruption. *Nature*, 609(7928), 741–746. https://doi.org/10.1038/s41586-022-05012-5
- Zhang, S.-R., Vierinen, J., Aa, E., Goncharenko, L. P., Erickson, P. J., Rideout, W., et al. (2022). 2022 Tonga volcanic eruption induced global propagation of ionospheric disturbances via lamb waves. Frontiers in Astronomy and Space Sciences, 9. https://doi.org/10.3389/fspas.2022.871275

ZHANG ET AL. 9 of 9